Title

Evaluation of predictive models of aneurysm focal growth and bleb development using machine learning techniques.

Journal

Journal of NeuroInterventional Surgery, 16(4)

Authors

Hadad, Sara
Mut, Fernando
Slawski, Martin
et al.

Publication Date

2024-03-14

DOI

10.1136/jnis-2023-020241

Peer reviewed

HHS Public Access

Author manuscript

J Neurointerv Surg. Author manuscript; available in PMC 2024 March 18.

Published in final edited form as:

J Neurointerv Surg. ; 16(4): 392–397. doi:10.1136/jnis-2023-020241.

Evaluation of Predictive Models of Aneurysm Focal Growth and Bleb Development Using Machine Learning Techniques

Sara Hadad[1], **Fernando Mut**[1], **Martin Slawski**[2], **Anne M Robertson**[3,4], **Juan R Cebral**[1,5]

[1]Department of Bioengineering George Mason University, Fairfax, VA, USA

[2]Statistics Department, George Mason University, Fairfax, VA, USA

[3]Department of Mechanical Engineering and Material Science, University of Pittsburgh, Pittsburgh, Pennsylvania, USA

[4]Department of Bioengineering, University of Pittsburgh, Pittsburgh, Pennsylvania, USA

[5]Department of Mechanical Engineering George Mason University, Fairfax, VA, USA

Abstract

Background: Since bleb presence increases the rupture risk of intracranial aneurysms (IAs), this study aimed to evaluate whether cross-sectional bleb formation models can identify aneurysms with focalized enlargement in longitudinal series.

Methods: Hemodynamic, geometric, and anatomical variables derived from computational fluid dynamics models of 2265 IAs from a cross-sectional dataset were used to train machine learning (ML) models for bleb development. ML algorithms, including logistic regression, random forest, bagging method, support vector machine, and k-nearest neighbors, were validated using an independent cross-sectional dataset of 266 IAs. The models' ability to identify aneurysms with focalized enlargement was evaluated using a separate longitudinal dataset of 174 IAs. Model performance was quantified by the area under the receiving operating characteristic curve (AUC), the sensitivity and specificity, positive predictive value, negative predictive value, F1 score, balanced accuracy, and misclassification error.

Results: The final model, with 3 hemodynamic and 4 geometrical variables, along with aneurysm location and morphology, identified strong inflow jets, nonuniform wall shear stress with high peaks, larger sizes, and elongated shapes as indicators of a higher risk of focal growth over time. The logistic regression model demonstrated the best performance on the longitudinal

Corresponding author: Sara Hadad, shadad@gmu.edu, Mailing address: 85 Rio Robles E, Apt 1432, San Jose, 95134, CA, USA.

Contributors: SH and JRC designed the study. SH and FM contributed to development of the methodology. FM and JRC designed the software tools. SH and JRC identified focal growing aneurysms in the dataset. SH curated the data. SH and MS performed the data analysis. SH, FM, MS, and JRC contributed to the interpretation of the results. AMR and JRC acquired funding, supervised students, and coordinated the project. SH and JRC drafted the manuscript. All authors contributed to the manuscript edition and approved the final manuscript.

Competing interests: None declared.

Ethics approval: The protocols for patient consent, handling of patient data, and analysis were approved by the institutional review board (IRB) at the University of Pittsburgh (Protocol # STUDY20020015). The whole study's IRB is overseen by the University of Pittsburgh and George Mason University.

series, achieving an AUC of 0.9, sensitivity of 85%, specificity of 75%, balanced accuracy of 80%, and a misclassification error of 21%.

Conclusions: Models trained with cross-sectional data can identify aneurysms prone to future focalized growth with good accuracy. These models could potentially be used as early indicators of future risk in clinical practice.

1. INTRODUCTION

Intracranial aneurysms (IAs) may have an additional bulge in the wall called a bleb (1), which constitutes a significant risk factor for rupture, as many ruptured aneurysms are found to have blebs (2–4). Previous studies have suggested that irregular aneurysm shape, characterized by a multilobulated shape and the presence of blebs, is considered the most clinically relevant risk factor in practice (3,5). In fact, it is considered even more important than size. For instance, the risk score reported by unruptured intracranial aneurysm treatment score (UIATS) (6) is 3 for aneurysms with blebs, while it is 2 for aneurysms with diameter of 7 to 12.9 mm, and 1 for aneurysms with size ratio larger than 3. Therefore, aneurysms that experience focalized enlargement and develop new blebs or local irregularities undergo a considerable increase in their rupture potential. Furthermore, it has been shown that growing aneurysms have a much higher rupture rate than stable aneurysms (3.1% for growing aneurysms compared to 0.1% for stable aneurysms (5), and growing aneurysms have risk score of 4 in UIATS scale (6)). As such, it is important to identify early on those aneurysms that are prone to focalized growth and/or bleb development to recommend careful monitoring or treatment.

In 2003, Steinman et al. first reported the use of patient-specific geometry models in computational fluid dynamics (CFD) to analyze intracranial aneurysms (7). Subsequent CFD-based studies have highlighted the pivotal role of hemodynamics in understanding aneurysm pathology, encompassing initiation, growth, and rupture. For instance, wall shear stress (WSS) emerged as a key factor influencing bleb development, aneurysm initiation, growth, and rupture (12–15). Cebral et al.'s research indicated that increased WSS in specific areas contributed to localized wall damage leading to bleb formation (15). More recently, Ashkezari et al. proposed that the formation of blebs in aneurysms is facilitated by strong inflow jets and heterogeneous WSS patterns (16). Sforza et al. showed that growing aneurysms exhibit complex intrasaccular flow patterns that result in non-uniform WSS distributions, characterized by regions of high WSS concentration and large areas of low WSS (17).

Previous studies have identified associations between geometric, hemodynamic, and anatomical characteristics of IAs and the development of blebs (12,18). These characteristics have been proposed as potential inputs for statistical and machine learning (ML) models of bleb formation (19). However, the limited availability of large datasets of aneurysms followed longitudinally without treatment has made it challenging to develop such models, and previous studies have therefore relied on cross-sectional data of aneurysms imaged at a single point in time. Thus, the aim of this study was to evaluate the ability of bleb formation models constructed from cross-sectional data (including hemodynamic, geometrical, and

anatomical variables) to identify aneurysms that undergo focalized enlargement in a longitudinal dataset. This hypothesis is supported by the fact that similar associations between the geometric, hemodynamic, and anatomical characteristics of IAs have been observed in relation to both bleb development (12,20) and aneurysm growth (14,17,21–23).

2. METHODS

2.1. Datasets

From our database, cross-sectional data of 2265 aneurysms from several populations (USA, Europe other than Finland, and Japan) which were imaged with 3D rotational angiography (3DRA) and modeled with CFD were used to develop ML models of bleb development (training set). The ML models were validated with cross-sectional data of 266 IAs also imaged with 3DRA (validation set) from an independent cohort. These datasets are described in detail in previous reports (19,24). Subsequently, a total of 174 aneurysms that were followed up over time without treatment using 3DRA, computed tomography angiography (CTA), or magnetic resonance angiography (MRA) were used to evaluate if these ML models were able to identify aneurysms that grew focally or developed blebs during the follow up observation (longitudinal test set). All data was anonymized before storage into our database and analysis, and the study was approved by our IRB.

The aneurysms in the cross-sectional datasets (training and validation sets) were divided into two subsets: aneurysms with blebs and aneurysms without blebs. As in previous studies, blebs were identified as secondary well-defined focal bulges by inspection of the 3D images (18). Similarly, aneurysms in the longitudinal test set were divided into two subsets: stable aneurysms (no appreciable change during follow up) and aneurysms with focal growth (local expansion of more than 0.5 mm during follow up – this threshold, which is larger than the typical imaging resolution, has routinely been used clinically to identify growing aneurysms). The number of aneurysms based on their location (ACA, ACOMA, BA, ICA, MCA, PCOMA, PICA), morphology (Lateral or Bifurcation), label (Bleb/focal growing or No-bleb/stable), and the mean aneurysms size for each group are given in Supplementary Table 1.

2.2. Aneurysm Modeling and Characterization

Using a previously described approach (25), patient-specific 3D models were constructed from the 3D images (3DRA, CTA, or MRA) using a combination of image filtering (e.g. median filter to eliminate noise), threshold segmentation, and iso-surface extraction followed by non-shrinking smoothing. Arteries were cut perpendicularly to their axes to define inlet and outlet boundaries. Unstructured grids of (linear) tetrahedral elements with a minimum resolution of 0.2 mm were generated with an advancing front method (26), which resulted in meshes ranging from 3.5 to 10.5 million elements. Computational fluid dynamics (CFD) simulations were performed by numerically solving the incompressible unsteady Navier-Stokes equations using a fully implicit finite elements scheme (27,28). A constant Newtonian viscosity of $\mu = 0.04\ g/cm.\ s$ and a blood density of $\rho = 1.0\ g/cm^3$ were used. Since the maximum Reynolds numbers were below 800 a laminar flow assumption was deemed reasonable. All simulation software and quantification tools were developed

in-house and have been verified and validated over a wide range of applications over the years (29). Pulsatile inflow conditions at the inlets in the internal carotid or vertebral arteries were prescribed by scaling representative waveforms with an empirical power-law of the vessel diameter derived from flow measurements in a patient population (30), i.e. although not measured directly on each patient, flow conditions were individualized by scaling with the patient-specific inlet vessel diameter. Outflow conditions consistent with Murray's law were applied, and vessel walls were approximated as non-compliant (31). Simulations were performed for 2 cardiac cycles with time steps of 0.01 sec and the flow fields of the second cycle were used to quantify the aneurysm hemodynamics. Each aneurysm was characterized by a number of hemodynamics and geometrical variables previously described (27,32), as well as anatomical characteristics (location, morphology, multiplicity). Previous work showed that the choice of simulation parameters (timestep, number of cardiac cycles, etc.) and approximations (Newtonian fluid, rigid walls, etc.) described above is appropriate to quantify these hemodynamic variables (33).

2.3. Aneurysm Labeling

Aneurysms in the cross-sectional datasets that harbored blebs were identified visually guided by the aneurysm Gaussian curvature as described in detail by Salimi Ashkezari et al. (18). To approximate the hemodynamics and geometrical characteristics of these aneurysms prior to bleb development, the blebs were virtually deleted from the reconstructed vascular models and CFD simulations were performed for the 3D models with their blebs removed as described in the previous study (12).

Aneurysms in the longitudinal dataset that exhibited focalized growth or bleb development during follow up were identified by measuring the local aneurysm enlargement (17). To measure this enlargement, a previously developed tool (cheAlignSurf) (34) was used to interactively align the 3D vascular model of the last follow-up to the 3D model of the initial examination (baseline) making sure the parent arteries coincided as much as possible (Fig1.E), i.e. minimizing the distance between the parent arteries in the vicinity of the aneurysm. Then, the region of the aneurysm where the distance between the two aligned vascular models was larger than 0.5 mm was determined from the distance map between the two aligned vascular surfaces (34) and was labeled (painted) as the growing region on the baseline model (Fig.1 F). Aneurysms that did not enlarge more than 0.5 mm were labeled as stable (17), and aneurysms that exhibited uniform or global growth (enlargement of the entire sac) were excluded. Fig.1 shows an example of a focal growing aneurysm and illustrates the methodology to identify aneurysms with focal growth. Fig1.B and D show the 3D models of the baseline and the last follow-up of the aneurysm, respectively. All aneurysm features used in this study (cross-sectional and longitudinal datasets) were based on the CFD simulations of the baseline geometry since the purpose of this study was to develop predictive models for future aneurysm growth or bleb development.

2.4. Development of Predictive Models of Bleb Formation

Several supervised machine learning binary classifier models, including logistic regression (LR), random forest (RF), bagging or bootstrap aggregating method (BG), support vector machine (SVM), and K-nearest neighbors (KNN), were used to build predictive models

of bleb development/focal growth. The models were based on 22 hemodynamic features (including the average number of critical points in the WSS field described by Salimi Ashkezari et al. (12)) and 25 geometrical features described in Detmer et al. (35), and 3 anatomical characteristics of the aneurysms and patient population. These predictor characteristics included continuous and categorical variables. The categorical variables (aneurysm location, morphology, multiplicity, and population) were encoded as dummy variables. The continuous variables were standardized so that their means and standard deviation equal zero and one respectively. For all the aneurysms, all the predictor variables were available (i.e., no missing data). A complete list of variables used in this study is provided in Supplementary Table 2. As explained earlier, cross-sectional data was used to train ML models of bleb development. To estimate the associated tuning parameters and train the models, tenfold cross-validation with 100 repetitions was used. In this step, the training set was randomly split into two subsets, a training subset and a testing subset, for each of the ten folds. The average area under the curve (AUC) of the receiver operating characteristics (ROC) in the test subsets was obtained through a grid search and was used to determine the optimal values of the tuning parameters during model training.

Since only 32% of aneurysms in the training set and 35% of them in the validation set were identified as harboring blebs, these datasets were inherently unbalanced. To minimize the negative effect of imbalanced data, during the internal cross-validation a down-sampling approach was used in which data with the majority class were randomly removed to balance the class distribution.

2.5. Feature Selection

To select parsimonious sets of predictors, first variables that were highly correlated to other variables (absolute correlation of 0.75 or higher) were removed. Moreover, variables were ranked based on their variables inflation factor (VIF), from highest to lowest magnitude, and multicollinear variables with a VIF of 10 or larger were removed one at a time (the one with highest VIF first) in a recursive manner until all multicollinear variables were eliminated. The importance of the remaining variables was computed by measuring the increase in prediction error after permuting the variables. The less change in the model error, the lower the importance of the variable. The least important variables were removed one at a time while maintaining the model accuracy measured by the balanced accuracy. The iterative process continued until the balanced accuracy began to decrease, and subsequently a “brute force” approach was used to select the optimal subset of features by investigating all possible subsets that could be constructed with the retained variables. The optimal set of features was selected based on the model with the highest AUC in the validation set.

2.6. Validation of Bleb Formation Models

The different ML models of bleb development were validated with the cross-sectional data of the validation set (266 aneurysms). To quantify their performance, the AUC of the ROC, the sensitivity, specificity, positive predictive value (PPV), negative predictive value (NPV), F1 score, balanced accuracy, and the misclassification error were calculated and the model with the best overall performance was selected. The 95% confidence intervals of AUC were calculated using 2000 bootstrap iterations.

2.7. Evaluation of Models' Ability to Identify Aneurysms with Focal Growth

To evaluate the ability of the ML models trained with cross-sectional data to discriminate between aneurysms that exhibited focalized growth or bleb development and those that remained stable during follow up, the AUC of the ROC, the sensitivity (true positive rate), the specificity (true negative rate), positive predictive value (PPV), negative predictive value (NPV), F1 score, balanced accuracy, and the misclassification error were calculated for the ML models using the longitudinal test set.

3. RESULTS

3.1. Variables Retained in the Model

Supplementary Table 2 lists the 51 variables considered in this study, along with their mathematical definitions and references. After removing correlated variables, 25 variables remained. The initial importance of these 25 variables, assessed on the validation set, is presented in Supplementary Fig. 1. Supplementary Fig. 2 demonstrates a gradual decline in accuracy after eliminating the 6 least important variables. Subsequently, a "brute force" method was employed to investigate all possible models using the 19 remaining features (the most important variables) in order to identify the optimal subset for developing predictive models. The final model, with the highest AUC, included 9 variables: mean aneurysm inflow rate (Q), maximum normalized wall shear stress (MWSSnorm), size ratio (SizR), volume to ostium ratio (VOR), non-sphericity index (NSI), convexity ratio (CR), location, morphology, and proper orthogonal decomposition entropy (podent). These variables were used consistently across all ML models. Supplementary Fig. 3 displays the importance of the retained variables in the final model, listed in descending order of importance.

3.2. Model Validation

The logistic regression model had the best performance in validation (using the cross-sectional validation set) with AUC of 0.77, sensitivity of 0.85, specificity of 0.61, balanced accuracy of 0.74, and misclassification error of 0.30. Table 1. presents the performance results for the logistic regression as well as the other ML models. The corresponding ROC curves are shown in Supplementary Fig. 4.

3.3. Performance of Predictive Models on Longitudinal Data

The logistic regression model demonstrated the best performance among the ML models when evaluated on both the cross-sectional validation set and the longitudinal test set. Table 2. presents the model's results on the longitudinal dataset, with an AUC of 0.90, sensitivity of 0.85, specificity of 0.75, balanced accuracy of 0.80, and a misclassification error of 0.21. Supplementary Fig. 5 displays the ROC curve depicting the performance of different models on the longitudinal data.

Fig. 2 showcases examples of aneurysms from the longitudinal dataset correctly classified by the LR model. The top panel presents three examples of focal growth aneurysms at baseline, ranging from large to small sizes, while the bottom panel displays three stable aneurysms with similar sizes. The top row visualizes the inflow jet, and the bottom row shows the WSS distribution at peak systole. Supplementary Table 3. provides further details

on these example aneurysms. Focally growing aneurysms exhibit strong inflow jets and elevated WSS, with the LR model assigning them growth probabilities of 95%, 94%, and 84%. Stable aneurysms display more diffuse inflow jets, lower WSS distributions, and were assigned stability probabilities of 78%, 86%, and 90% by the LR model. These examples demonstrate how the ML model, combining hemodynamic, geometric, and anatomical information, aids in identifying aneurysms prone to focal growth and bleb development, thus increasing their rupture risk.

4. DISCUSSION

Previous studies have shown that aneurysm hemodynamic, geometric, and anatomical characteristics are associated with bleb presence (15,17,36). In particular, aneurysms that are prone to bleb development tend to have larger inflow rates, higher WSS, wider necks, and more elongated shapes than those that are less likely to develop blebs (15,17,36). However, these studies were conducted with cross-sectional data. Similar associations have also been found between these aneurysm characteristics (along with location) and aneurysm growth (17,22,23,37). Therefore, the goal of this study was to test if predictive models of bleb formation constructed from cross-sectional data could be used to identify aneurysms that are prone to future focalized growth or bleb development.

It was found that the predictive models of bleb formation developed in this study, using cross-sectional data, were indeed able to identify aneurysms that grew focally in a longitudinal dataset with 85% sensitivity However, there was a 25% misclassification of stable aneurysms as being at risk of future focal growth.

While these models accurately detect problematic aneurysms likely to experience focalized growth, they may also misclassify stable aneurysms due to various reasons. One possibility is that aneurysms classified as having a high probability of focal growth but considered stable could grow if observed for a longer follow-up period. For instance, in Supplementary Fig. 6, an aneurysm remained stable for three years but grew after five years from the initial examination. Initially, according to our stability definition (no increase > 0.5mm in any direction), the aneurysm showed stability (Supplementary Fig. 6.A). However, subsequent follow-up studies conducted five and ten years later revealed growth (Supplementary Fig. 6.B and C). Our dataset labeled this aneurysm as having focal growth since we considered the baseline (the initial examination) and the last follow-up (ten years after the initial examination), correctly classified by the LR model. Nonetheless, had the follow-up ended three years after the initial examination, the aneurysm would have been misclassified as stable by the LR model. This underscores the need for longitudinal datasets with extended follow-up periods to consistently label stable aneurysms.

Interestingly, in our study, the logistic regression model outperformed the other more sophisticated ML models when evaluated on the longitudinal dataset. While the exact reasons for this are not clear, it seems that the LR model was able to better capture the key relationships between the variables in the longitudinal set, which may be have been simpler than in the cross-sectional sets, thus making the LR model better suited for generalizing its application to different datasets.

The LR model identifies key predictors indicating a higher likelihood of focal growth in aneurysms compared to stable ones. These predictors include larger inflow rates (Q), unstable flows (podent), heterogeneous wall shear stress distributions with more critical points and higher peaks (MWSSnorm), larger size (SR), and greater elongation (NSI, VOR). Aneurysm location and morphology also contribute to the potential for focalized growth. While it is challenging to pinpoint a single factor responsible for growth and bleb development, the adverse biomechanical environment encompassing these features likely adversely affects the aneurysm wall, predisposing it to future focal growth. Investigating cellular responses in relation to local biomechanical conditions in future studies may reveal the exact mechanisms driving local wall degeneration and bleb formation.

Naturally, predictive models of focalized growth could be trained directly with longitudinal data, which are expected to yield a better overall accuracy. However, collecting large longitudinal datasets is more challenging as many aneurysms are treated instead of conservatively observed. Nevertheless, our study demonstrated that models trained on cross-sectional data can identify the aneurysms most likely to develop focal growth (and possibly blebs), thus becoming more irregular in shape and consequently increasing their rupture risk. Moreover, the risk associated with treating incidentally discovered aneurysms to prevent subarachnoid hemorrhage often outweighs their natural rupture risk, which is approximately 1% per year (38–40). With the increased use of medical imaging, the number of detected unruptured aneurysms has gone up, leading to more frequent treatment decisions. Therefore, it is essential to identify aneurysms that are likely to grow in the future and limit initial treatment recommendations to only those cases (38–41). Thus, our study's approach serves as an early indicator of future risk, aiding in treatment selection or more frequent and attentive observation of such aneurysms.

There are several limitations to consider in this study. Firstly, our CFD models rely on assumptions such as Newtonian flow, non-patient-specific laminar viscosity, rigid walls, estimated inflow rates, and limited cardiac cycle simulations. While previous studies suggest these approximations have minimal impact on computed hemodynamic variables used as predictors for focalized growth (33,42), their influence should still be acknowledged. Secondly, limitations are associated with the study itself. In the training and validation sets, we estimated the hemodynamics and geometric features of aneurysms by virtually removing blebs. This assumes rapid bleb development while parent aneurysms remain relatively unchanged, supported by longitudinal observations. The imbalanced datasets (few aneurysms with blebs or focal growth) require careful consideration. We used a downsampling approach, which reduces sample sizes and imposes accuracy limits on the models. The small sample size of the longitudinal dataset, short follow-up times for labeling stable aneurysms, and differing selection biases between the cross-sectional training set and longitudinal test sets may result in decreased accuracy when transferring statistical models across domains. The alignment of baseline and follow-up vascular models was done interactively, and the threshold for identifying aneurysm enlargement was set to 0.5 mm. Altering these parameters or the manual process could impact results and are considered limitations. Nonetheless, despite these limitations, the model demonstrated reasonably good performance, indicating potential for clinical application after further evaluation with larger longitudinal datasets.

5. CONCLUSIONS

Predictive models of bleb formation based on cross-sectional data can identify aneurysms prone to focalized growth in longitudinal datasets. These models could potentially be used as early indicators of future risk in intracranial aneurysms.

Supplementary Material

Refer to Web version on PubMed Central for supplementary material.

Funding:

This work was supported by the NIH grants 2R01NS097457, and R01NS121286.

REFERENCES

1. Mori K, Watanabe S, Nakao Y, Yamamoto T, Toyooka T, Wada K. Complex and continuous change in hypothetic risk of rupture of intracranial cerebral aneurysms – Bleb mandala –. Interdiscip Neurosurg. 2021 Sep 1;25:101221.
2. Burkhardt JK, Fierstra J, Esposito G, Baltsavias G, Bozinov O, Regli L. Rapid Documented Growth of Aneurysm Bleb Led to Rupture of an Incidental Intracranial Anterior Communicating Artery Aneurysm. J Neurol Surg Part Cent Eur Neurosurg. 2017 Sep;78(5):521–4.
3. Lindgren AE, Koivisto T, Björkman J, von Und Zu Fraunberg M, Helin K, Jääskeläinen JE, et al. Irregular Shape of Intracranial Aneurysm Indicates Rupture Risk Irrespective of Size in a Population-Based Cohort. Stroke. 2016 May;47(5):1219–26. [PubMed: 27073241]
4. Yamano A, Yanaka K, Uemura K, Onuma K, Nakamura K, Ishikawa E. Bleb formation in small unruptured intracranial aneurysm as a predictor of early rupture. J Surg Case Rep. 2018 May 1;2018(5):rjy117. [PubMed: 29977511]
5. Brinjikji W, Zhu YQ, Lanzino G, Cloft HJ, Murad MH, Wang Z, et al. Risk Factors for Growth of Intracranial Aneurysms: A Systematic Review and Meta-Analysis. AJNR Am J Neuroradiol. 2016 Apr;37(4):615–20.
6. Etminan N, Brown RD, Beseoglu K, Juvela S, Raymond J, Morita A, et al. The unruptured intracranial aneurysm treatment score. Neurology. 2015 Sep 8;85(10):881–9. [PubMed: 26276380]
7. Steinman DA, Milner JS, Norley CJ, Lownie SP, Holdsworth DW. Image-based computational simulation of flow dynamics in a giant intracranial aneurysm. AJNR Am J Neuroradiol. 2003 Apr;24(4):559–66. [PubMed: 12695182]
8. Mantha A, Karmonik C, Benndorf G, Strother C, Metcalfe R. Hemodynamics in a Cerebral Artery before and after the Formation of an Aneurysm. AJNR Am J Neuroradiol. 2006 May;27(5):1113–8. [PubMed: 16687554]
9. Sforza DM, Putman CM, Cebral JR. Computational fluid dynamics in brain aneurysms. Int J Numer Methods Biomed Eng. 2012 Jun;28(0):801–8.
10. Murayama Y, Fujimura S, Suzuki T, Takao H. Computational fluid dynamics as a risk assessment tool for aneurysm rupture. Neurosurg Focus. 2019 Jul 1;47(1):E12.
11. Rahma AG, Abdelhamid T. Hemodynamic and fluid flow analysis of a cerebral aneurysm: a CFD simulation. SN Appl Sci. 2023 Jan 24;5(2):62.
12. Salimi Ashkezari SF, Mut F, Chung BJ, Robertson AM, Cebral JR. Hemodynamic conditions that favor bleb formation in cerebral aneurysms. J Neurointerventional Surg. 2021 Mar;13(3):231–6.
13. Diagbouga MR, Morel S, Bijlenga P, Kwak BR. Role of hemodynamics in initiation/growth of intracranial aneurysms. Eur J Clin Invest. 2018;48(9):e12992. [PubMed: 29962043]
14. Dabagh M, Nair P, Gounley J, Frakes D, Gonzalez LF, Randles A. Hemodynamic and morphological characteristics of a growing cerebral aneurysm. Neurosurg Focus. 2019 Jul 1;47(1):E13.

15. Cebral JR, Sheridan M, Putman CM. Hemodynamics and bleb formation in intracranial aneurysms. AJNR Am J Neuroradiol. 2010 Feb;31(2):304–10. [PubMed: 19797790]
16. Ashkezari SFS, Mut F, Chung BJ, Robertson AM, Cebral JR. Hemodynamic conditions that favor bleb formation in cerebral aneurysms. J NeuroInterventional Surg. 2021 Mar 1;13(3):231–6.
17. Sforza DM, Kono K, Tateshima S, Viñuela F, Putman C, Cebral JR. Hemodynamics in growing and stable cerebral aneurysms. J Neurointerventional Surg. 2016 Apr;8(4):407–12.
18. Salimi Ashkezari SF, Detmer FJ, Mut F, Chung BJ, Yu AK, Stapleton CJ, et al. Blebs in Intracranial Aneurysms: Prevalence and General Characteristics. J Neurointerventional Surg. 2021 Mar;13(3):226–30.
19. Salimi Ashkezari SF, Mut F, Slawski M, Cheng B, Yu AK, White TG, et al. Prediction of bleb formation in intracranial aneurysms using machine learning models based on aneurysm hemodynamics, geometry, location, and patient population. J Neurointerventional Surg. 2022 Oct;14(10):1002–7.
20. Uno T, Misaki K, Futami K, Nambu I, Yoshikawa A, Kamide T, et al. Hemodynamic factor evaluation using computational fluid dynamics analysis for de novo bleb formation in unruptured intracranial aneurysms. Neurol Sci. 2022;43(3):1849–57. [PubMed: 34331615]
21. Boussel L, Rayz V, McCulloch C, Martin A, Acevedo-Bolton G, Lawton M, et al. Aneurysm growth occurs at region of low wall shear stress: patient-specific correlation of hemodynamics and growth in a longitudinal study. Stroke. 2008 Nov;39(11):2997–3002. [PubMed: 18688012]
22. Kimura H, Hayashi K, Taniguchi M, Hosoda K, Fujita A, Seta T, et al. Detection of Hemodynamic Characteristics Before Growth in Growing Cerebral Aneurysms by Analyzing Time-of-Flight Magnetic Resonance Angiography Images Alone: Preliminary Results. World Neurosurg. 2019 Feb;122:e1439–48. [PubMed: 30465954]
23. Chien A, Xu M, Yokota H, Scalzo F, Morimoto E, Salamon N. Nonsphericity Index and Size Ratio Identify Morphologic Differences between Growing and Stable Aneurysms in a Longitudinal Study of 93 Cases. AJNR Am J Neuroradiol. 2018 Mar;39(3):500–6. [PubMed: 29371255]
24. Detmer FJ, Fajardo-Jiménez D, Mut F, Juchler N, Hirsch S, Pereira VM, et al. External validation of cerebral aneurysm rupture probability model with data from two patient cohorts. Acta Neurochir (Wien). 2018 Dec;160(12):2425–34. [PubMed: 30374656]
25. Cebral JR, Castro MA, Appanaboyina S, Putman CM, Millan D, Frangi AF. Efficient pipeline for image-based patient-specific analysis of cerebral aneurysm hemodynamics: technique and sensitivity. IEEE Trans Med Imaging. 2005 Apr;24(4):457–67. [PubMed: 15822804]
26. Löhner R, Haug E, Michalski A, Muhammad B, Drego A, Nanjundaiah R, et al. Recent advances in computational wind engineering and fluid–structure interaction. J Wind Eng Ind Aerodyn. 2015 Sep 1;144:14–23.
27. Mut F, Löhner R, Chien A, Tateshima S, Viñuela F, Putman C, et al. Computational Hemodynamics Framework for the Analysis of Cerebral Aneurysms. Int J Numer Methods Biomed Eng. 2011 Jun 1;27(6):822–39.
28. Cebral JR, Yim PJ, Löhner R, Soto O, Choyke PL. Blood Flow Modeling in Carotid Arteries with Computational Fluid Dynamics and MR Imaging. Acad Radiol. 2002 Nov 1;9(11):1286–99. [PubMed: 12449361]
29. Applied CFD Techniques: An Introduction Based on Finite Element Methods - Löhner, Rainald: 9780471498438 - AbeBooks [Internet]. [cited 2023 May 7]. Available from: https://www.abebooks.com/9780471498438/Applied-CFD-Techniques-Introduction-Based-0471498432/plp
30. Durka MJ, Wong IH, Kallmes DF, Pasalic D, Mut F, Jagani M, et al. A data-driven approach for addressing the lack of flow waveform data in studies of cerebral arterial flow in older adults. Physiol Meas. 2018 Feb 1;39(1):015006. [PubMed: 29205172]
31. Sherman TF. On connecting large vessels to small. The meaning of Murray's law. J Gen Physiol. 1981 Oct;78(4):431–53. [PubMed: 7288393]
32. Ma B, Harbaugh RE, Raghavan ML. Three-dimensional geometrical characterization of cerebral aneurysms. Ann Biomed Eng. 2004 Feb;32(2):264–73. [PubMed: 15008374]

33. Cebral JR, Duan X, Gade PS, Chung BJ, Mut F, Aziz K, et al. Regional Mapping of Flow and Wall Characteristics of Intracranial Aneurysms. Ann Biomed Eng. 2016 Dec;44(12):3553–67. [PubMed: 27350071]
34. Cebral JR, Mut F, Gade P, Cheng F, Tobe Y, Frosen J, et al. Combining Data from Multiple Sources to Study Mechanisms of Aneurysm Disease: Tools and Techniques. Int J Numer Methods Biomed Eng. 2018 Nov;34(11):e3133.
35. Detmer FJ, Chung BJ, Mut F, Slawski M, Hamzei-Sichani F, Putman C, et al. Development and internal validation of an aneurysm rupture probability model based on patient characteristics and aneurysm location, morphology, and hemodynamics. Int J Comput Assist Radiol Surg. 2018 Nov;13(11):1767–79. [PubMed: 30094777]
36. Tateshima S, Murayama Y, Villablanca JP, Morino T, Nomura K, Tanishita K, et al. In vitro measurement of fluid-induced wall shear stress in unruptured cerebral aneurysms harboring blebs. Stroke. 2003 Jan;34(1):187–92. [PubMed: 12511772]
37. Shakur SF, Alaraj A, Mendoza-Elias N, Osama M, Charbel FT. Hemodynamic characteristics associated with cerebral aneurysm formation in patients with carotid occlusion. J Neurosurg. 2018 May 4;130(3):917–22. [PubMed: 29726778]
38. Wiebers DO. Unruptured intracranial aneurysms: natural history, clinical outcome, and risks of surgical and endovascular treatment. The Lancet. 2003 Jul 12;362(9378):103–10.
39. Juvela S, Poussa K, Lehto H, Porras M. Natural History of Unruptured Intracranial Aneurysms. Stroke. 2013 Sep;44(9):2414–21. [PubMed: 23868274]
40. UCAS Japan Investigators, Morita A, Kirino T, Hashi K, Aoki N, Fukuhara S, et al. The natural course of unruptured cerebral aneurysms in a Japanese cohort. N Engl J Med. 2012 Jun 28;366(26):2474–82. [PubMed: 22738097]
41. Gabriel RA, Kim H, Sidney S, McCulloch CE, Singh V, Johnston SC, et al. Ten-Year Detection Rate of Brain Arteriovenous Malformations in a Large, Multiethnic, Defined Population. Stroke. 2010 Jan;41(1):21–6. [PubMed: 19926839]
42. Detmer FJ, Mut F, Slawski M, Hirsch S, Bijlenga P, Cebral JR. Incorporating variability of patient inflow conditions into statistical models for aneurysm rupture assessment. Acta Neurochir (Wien). 2020 Mar;162(3):553–66. [PubMed: 32008209]

What is already known on this topic?

The presence of blebs significantly increases the risk of rupture for intracranial aneurysms, and there is a limited availability of large datasets that track aneurysms longitudinally without treatment.

What this study adds?

Models trained on cross-sectional data can identify aneurysms that are likely to exhibit future focal growth with good accuracy.

How this study might affect research, practice or policy?

These models have the potential to be utilized as early warning signs of future risk in clinical settings.

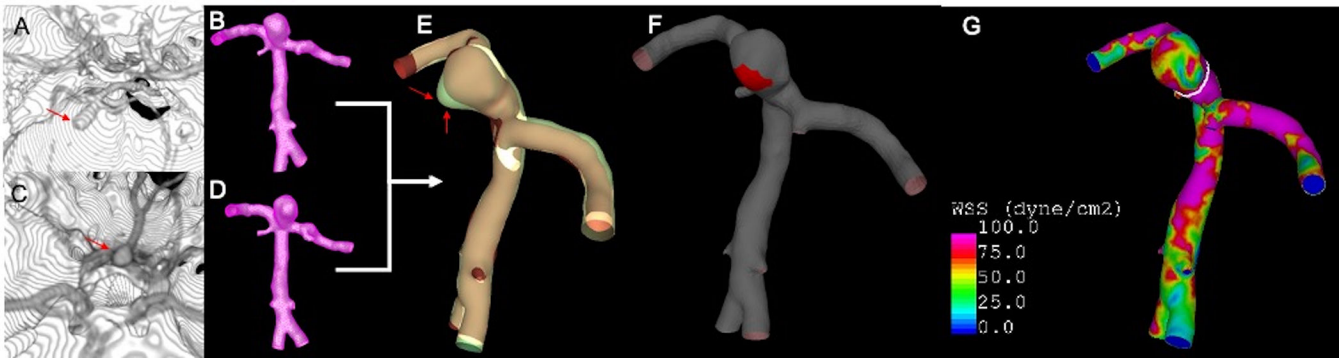

Figure 1:

Illustration of the methodology used to identify aneurysms with focal growth. Construction of a vascular model of basilar tip aneurysm from CTA images for the baseline image (A, B) and the last follow-up image (C, D). Model alignment (E) where the green transparent model represents the last follow-up model aligned with the baseline model (red model) and red arrows point to the growing region. The growing region painted on the baseline model (F) and CFD simulation (WSS distribution) of the baseline model (G).

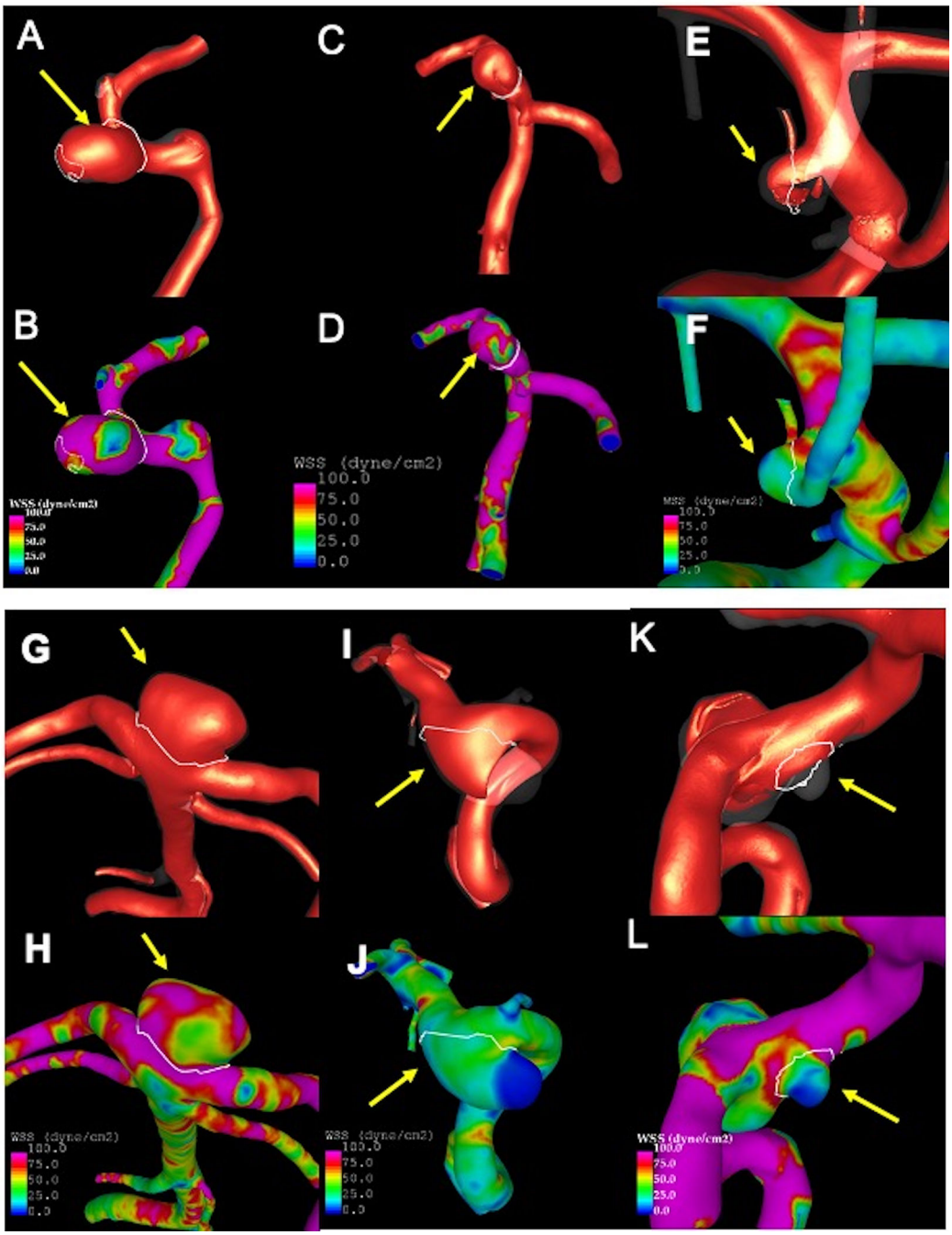

Figure 2.

Examples of aneurysms with focal growth (A-F) and stable aneurysms (G-L) that were classified correctly by the LR model. The first row of each panel shows the aneurysm inflow jet, and the second row shows the WSS, both at peak systole. In general, focally growing aneurysms had stronger inflow jets (A, C, E) and were exposed to high WSS (B, D) while stable aneurysms had weaker inflow jets (K) and lower WSS (H, L).

Table 1.

Performance of different ML models applied to the cross-sectional validation set

Model	AUC	Sensitivity	Specificity	PPV	NPV	F1 Score	Balanced accuracy	Misclassification
LR	0.77	0.85	0.61	0.55	0.88	0.67	0.74	0.30
RF	0.75	0.88	0.54	0.51	0.89	0.65	0.71	0.34
BG	0.74	0.75	0.60	0.51	0.81	0.61	0.67	0.35
SVM	0.77	0.86	0.53	0.51	0.87	0.64	0.70	0.35
KNN	0.70	0.85	0.51	0.49	0.86	0.63	0.68	0.36

Table 2.

Performance of different ML models applied to the longitudinal test set

Model	AUC	Sensitivity	Specificity	PPV	NPV	F1 Score	Balanced accuracy	Misclassification
LR	0.9	0.85	0.75	0.65	0.90	0.73	0.80	0.21
RF	0.68	0.58	0.68	0.49	0.76	0.53	0.63	0.35
BG	0.65	0.50	0.72	0.48	0.73	0.49	0.61	0.36
SVM	0.73	0.37	0.75	0.44	0.69	0.34	0.56	0.38
KNN	0.60	0.25	0.67	0.28	0.63	0.27	0.46	0.48